

Journal Pre-proof

i-Rheo-optical assay: Measuring the viscoelastic properties of multicellular spheroids

Rosalia Ferraro, Stefano Guido, Sergio Caserta, Manlio Tassieri



PII: S2590-0064(24)00125-X

DOI: <https://doi.org/10.1016/j.mtbio.2024.101066>

Reference: MTBIO 101066

To appear in: *Materials Today Bio*

Received Date: 8 February 2024

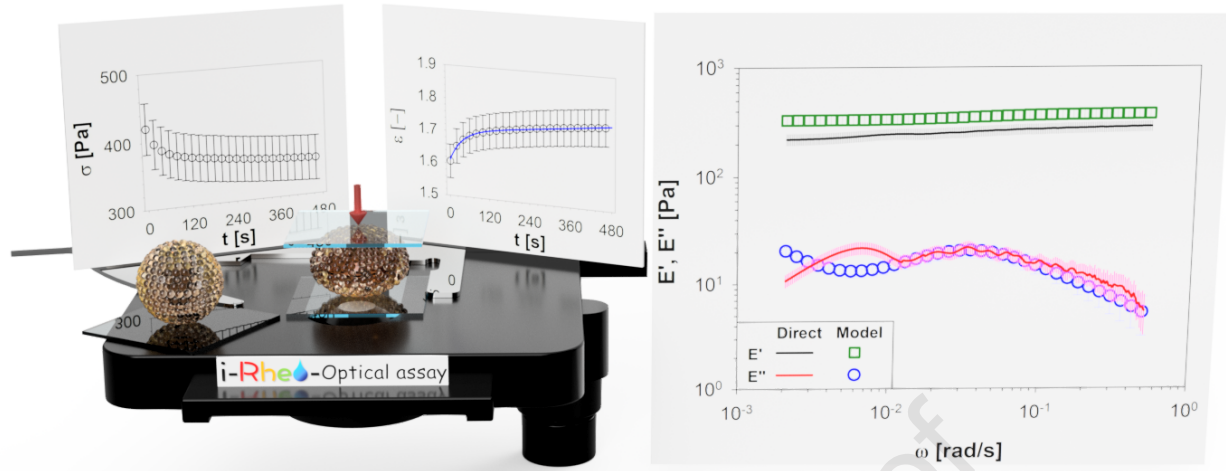
Revised Date: 15 April 2024

Accepted Date: 18 April 2024

Please cite this article as: R. Ferraro, S. Guido, S. Caserta, M. Tassieri, *i*-Rheo-optical assay: Measuring the viscoelastic properties of multicellular spheroids, *Materials Today Bio*, <https://doi.org/10.1016/j.mtbio.2024.101066>.

This is a PDF file of an article that has undergone enhancements after acceptance, such as the addition of a cover page and metadata, and formatting for readability, but it is not yet the definitive version of record. This version will undergo additional copyediting, typesetting and review before it is published in its final form, but we are providing this version to give early visibility of the article. Please note that, during the production process, errors may be discovered which could affect the content, and all legal disclaimers that apply to the journal pertain.

© 2024 Published by Elsevier Ltd.



i-Rheo-optical assay: Measuring the viscoelastic properties of multicellular spheroids

Rosalia Ferraro^{1,2}, Stefano Guido^{1,2}, Sergio Caserta^{1,2,†,*}, Manlio Tassieri^{3,†,**}

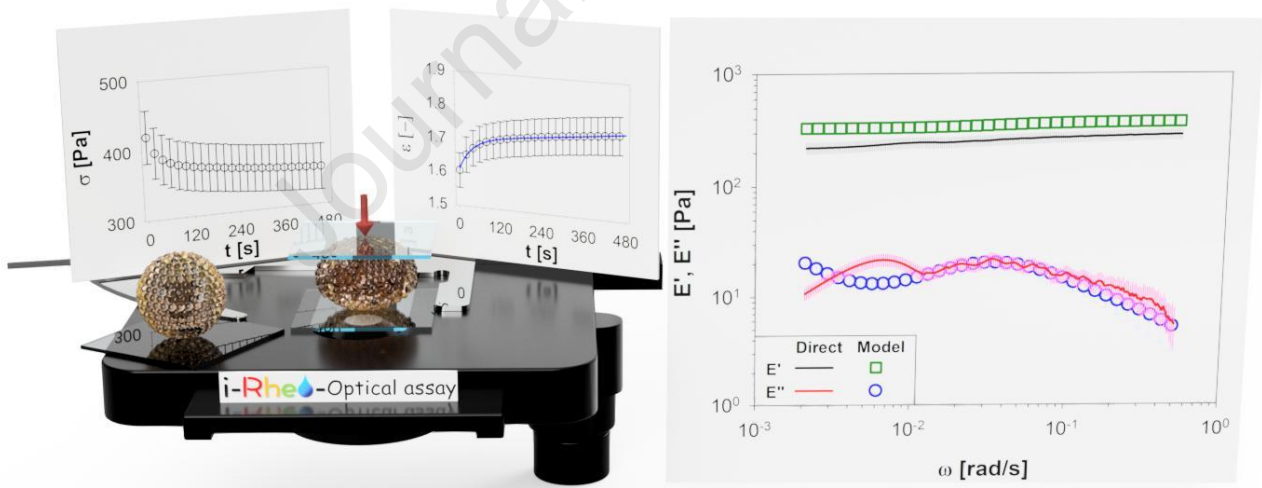
¹DICMaPI, Università di Napoli Federico II, P.le V. Tecchio 80, 80125 Napoli, Italy

²CEINGE Advanced Biotechnologies, Via Gaetano Salvatore, 486, 80131 Napoli, Italy

³Division of Biomedical Engineering, James Watt School of Engineering, Advanced Research Centre, University of Glasgow, Glasgow, G11 6EW, UK

† SC and MT contributed equally to this work.

Correspondence should be addressed to: (*) sergio.caserta@unina.it (SC), (**) manlio.tassieri@glasgow.ac.uk (MT)



Abstract

This study introduces a novel mechanobiology assay, named “i-Rheo-optical assay”, that integrates rheology with optical microscopy for analysing the viscoelastic properties of multicellular spheroids. These spheroids serve as three-dimensional models resembling tissue structures. The innovative technique enables real-time observation and quantification of morphological responses to applied stress using a cost-effective microscope coverslip for constant compression force application. By bridging a knowledge gap in biophysical research, which has predominantly focused on the elastic properties while only minimally exploring the viscoelastic nature in multicellular systems, the i-Rheo-optical assay emerges as an effective tool. It facilitates the measurement of broadband viscoelastic compressional moduli in spheroids, here derived from cancer (PANC-1) and non-tumoral (NIH/3T3) cell lines during compression tests.

This approach plays a crucial role in elucidating the mechanical properties of spheroids and holds potential for identifying biomarkers to discriminate between healthy tissues and their pathological counterparts. Offering comprehensive insights into the biomechanical behaviour of biological systems, i-Rheo-optical assay marks a significant advancement in tissue engineering, cancer research, and therapeutic development.

Keywords

Multicellular spheroids

Rheology

Mechanobiology

Cancer research

Optical assay

1. Introduction

The mechanical characterization of biological specimens, ranging from individual cells to monolayer-cultured cells and complex tissues, has garnered substantial attention in recent scientific literature. This heightened interest is attributed to the broader scientific community's recognition that the mechanical properties of biologically relevant specimens hold the potential to serve as effective biomarkers, facilitating the discrimination between healthy tissues and their pathological counterparts. This discrimination is achieved through the provision of valuable information regarding the frequency-dependent mechanical properties of these specimens, which are intricately regulated by a diverse array of physiological processes encompassing fundamental events such as cell migration [1], wound healing [2, 3], and immune responses [4-6]. Moreover, they play pivotal roles in pathological scenarios, with particular emphasis on their involvement in the metastatic progression of cancer [7-9]. The elucidation of the mechanical properties associated with these biological processes may significantly contribute to our understanding of the underlying mechanisms governing health and disease.

Within the field of tissue engineering, the incorporation of multicellular spheroids has arisen as a crucial strategy to bridge the existing knowledge disparity between conventional two-dimensional cell cultures and animal models [10-15]. Multicellular spheroids, indeed, serve as a noteworthy surrogate for animal models, as they faithfully emulate the intricacies of the *in vivo* tissue microenvironment. Consequently, they provide a more accurate representation of biological responses [16-19]. The three-dimensional structures of multicellular spheroids facilitate robust cell-cell interactions, resulting in the establishment of tight junctions that closely resemble those observed in native tissues [10, 20-23]. This architectural feature enhances the physiological relevance of multicellular spheroids, contributing to their utility as an intermediate model system that captures aspects of tissue complexity beyond what is achievable in traditional two-dimensional cell cultures.

While the elastic properties of biological systems have garnered substantial attention across various fields, the viscoelastic nature of multicellular systems remains minimally explored in literature [24, 25]. Several experimental methodologies have been employed and customized for the investigation of these properties [26], including techniques such as atomic force microscopy (AFM) [27-30], indentation [28], tweezers [31], microfluidics [32-34], micropipettes [35, 36], osmotic compression [37], and confocal-rheology [38]. These methodologies are characterized by sophisticated apparatus and necessitate technical skills that may not be readily available.

In this work, we leverage cellular spheroids as a representative model for avascular early-stage tumours, acknowledging their capacity to yield invaluable insights into the nuanced rheological properties of these tumour-like structures. To conduct our study, we subjected spheroids derived from a cancer cell line, PANC-1, to a compression test. The liquid overlay technique was employed for spheroids preparation, selected for its judicious balance of cost-efficiency and ease of management [39, 40]. At the core of our rheo-optical compression assay was the utilization of a microscope coverslip to apply a constant load, resulting in the development of a cost-effective and user-friendly technique [41]. Essentially, our innovative approach produces strain-time curves of pivotal significance in elucidating the mechanical properties of the spheroids. Subsequently, data fitting of the resultant deformation was accomplished using a linear viscoelastic model, specifically the Burgers model [42, 43], to extract mechanical parameters such as the compressional elastic ($E'(\omega)$) and viscous ($E''(\omega)$) moduli. These parameters contribute to a comprehensive understanding of the rheological behaviour of the investigated cellular spheroids. Moreover, we employed the open-access, model-free executable tool named “i-Rheo” [44-46] to derive the viscoelastic properties of the samples directly from their time-dependent stress and strain curves and conducted comparisons with those obtained from the Burgers model. To corroborate our rheo-optical compression assay, we conducted a similar load test through nanoindentation measurements performed on PANC-1 spheroids and on two biomimetic hydrogels, designed for mimicking biological samples in terms of

their mechanical properties [11]. The primary aim of the additional investigation was to further validate the analytical procedure to derive the viscoelastic properties of hydrogels via i-Rheo by means of a comparative assessment with conventional oscillatory bulk-rheology measurements.

Following the successful validation of this methodology, the i-Rheo-optical assay was then applied to a second cell line, NIH/3T3, which served as the non-tumoral control. This was done to establish a robust and efficient tool for the swift assessment of viscoelastic moduli in biological systems across a broad frequency spectrum. This advancement holds significant promise for accelerating therapeutic investigations and gaining deeper insights into the mechanical behaviour of biological materials.

2. Materials and Methods

2.1. Cell culture and spheroid preparation

A fibroblast cell line derived from mouse NIH/Swiss embryos (short: NIH/3T3) and human pancreatic carcinoma cells (short: PANC-1) were cultured at a temperature of 37°C within a humidified environment containing 5% CO₂. This cultivation was conducted in 2D monolayers using their respective standard growth medium, which was made of Dulbecco's Modified Eagle's Medium (DMEM) supplemented with 10% (v/v) Fetal Bovine Serum (FBS), 1% (v/v) antibiotics (50 units/mL penicillin and 50 mg/mL streptomycin), and 1% (v/v) L-glutamine.

For the preparation of cellular spheroids from both cell lines, the classical liquid overlay technique [40, 47, 48] was employed. Each well of a 48-well plate (Nunclon Δ Multidishes, flat bottom, ThermoScientific, Nunc 150687) was coated with agarose gel (Ultrapure agarose, Invitrogen, Carlsbad, CA), which facilitates cell collection (at a density of $8 \cdot 10^3$ cells/well for NIH/3T3 and $3 \cdot 10^3$ cells/well for PANC-1) and the formation of cell-cell adhesions within the meniscus of the non-adhesive concave surface. Subsequently, the 48-well plate was incubated for approximately 7 days to achieve the formation of compact spheroids. For more information on the above process, the reader is referred to our previous publication [49].

2.2. Rheo-optical compression assay

The rheo-optical compression test was performed by means of microscopy glass coverslips used as stress loading probe on the cell spheroids sitting within standard 6-well plates. In particular, the cell spheroids were collected from the 48-well plate by using a pipette, and then placed into a 6-well plate containing approximately 3 mL of phosphate-buffered solution (PBS); thus, ensuring no wall effects and a consistent settling of the glass coverslip. For more information on the above process, the reader is referred to our recent publication [41].

During the compression test, images were acquired at a rate of 0.5Hz using an inverted microscope, i.e. an LSM 5 Pascal model by Carl Zeiss Advanced Imaging Microscopy in Jena, Germany. The entire experimental duration was eight minutes.

2.3. Image Analysis

To quantify the impact of mechanical stimuli on spheroid, the morphological changes of the cellular spheroids were assessed in terms of their area (A) and diameter (D) by using an image analysis routine developed with Image Pro Plus 6.0 by Media Cybernetics. The algorithm detected the diametral plane of the cellular spheroids for a total of 240 images for each spheroid of both cell lines.

The stress applied on a spheroid, $\sigma(t)$, was defined as $(F_w - F_A)/A_t$, where F_w represented the weight of the glass coverslips, F_A was the Archimedes force associated with the PBS in which the spheroid was placed, and A_t the diametral area of the spheroid measured at the current time. The applied stress was related to the deformation, defined as function strain, $\varepsilon(t)$. By assuming constant volume before and after compression, the strain was calculated as $\varepsilon(t) = h_t(t)/h_0 = (D_0/D_t(t))^2$, where $D(t)$ is the diameter of the spheroid as visualized from the compression direction, and $h(t)$ is the spheroid thickness along the direction of compression, i.e. the distance between the two confining glass surfaces. The indices '0' and 't' refer to the function values measured at times zero and current time, respectively. In this work, we approximated the spheroid's volume to that of an oblate spheroid,

characterized by three axes a , b , and c , where $a = b (= D) > c = h$, representing the spheroid's diameter and height, respectively.

2.4. Burgers model: from time- to frequency-domain

In the time-domain, in evaluating the viscoelastic properties of cellular spheroids, the correlation between stress ($\sigma(t)$) and strain ($\varepsilon(t)$) was subjected to fitting using the Burgers model [50] — a widely recognized model in the biomedical literature for characterizing the linear viscoelastic behaviour of complex materials, ranging from synthetic hydrogel to bone and tissues [42, 43, 51-57]. Burgers viscoelastic model combines a Maxwell model, *i.e.*, a spring and a dashpot in series, and Voigt model, *i.e.*, a spring in parallel with a dashpot, as schematically shown in **Figure 1**.

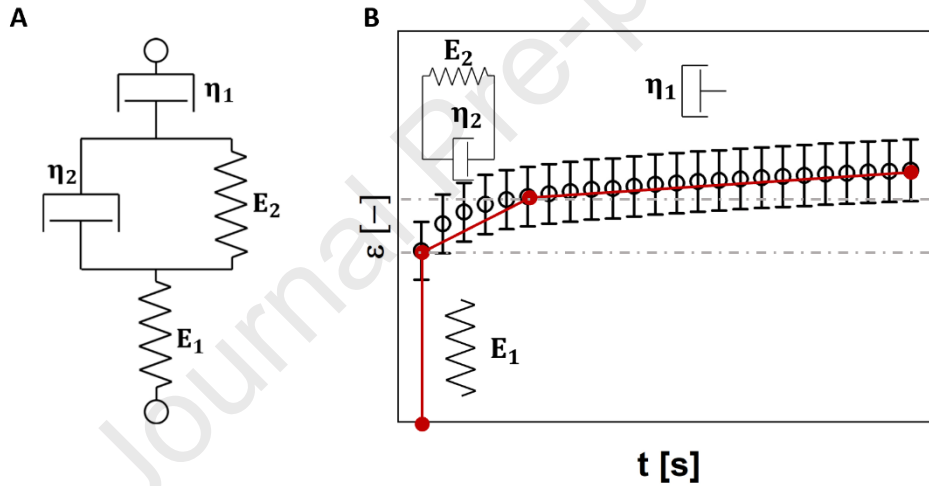


Figure 1. **A)** A schematic diagram of a Burgers material; **B)** A representation of the relative contributions of the individual components of a four-element Burgers model in a creep test, where the strain, ε , is drawn versus time, t .

The one-dimensional differential equation governing this model is expressed as follows:

$$\sigma(t) + \left(\frac{\eta_1}{E_1} + \frac{\eta_2}{E_1} + \frac{\eta_2}{E_2} \right) \dot{\sigma}(t) + \frac{\eta_1 \eta_2}{E_1 E_2} \ddot{\sigma}(t) = \eta_2 \dot{\varepsilon}(t) + \frac{\eta_1}{E_1} \eta_2 \ddot{\varepsilon}(t) \quad 1$$

Where $\sigma(t)$ is the axial stress loading, $\varepsilon(t)$ is the axial strain response, $\dot{\sigma}(t)$, $\ddot{\sigma}(t)$, $\dot{\varepsilon}(t)$, $\ddot{\varepsilon}(t)$, are their first and second time derivatives, respectively; while η_i and E_i are the viscous and the elastic coefficients of the Newtonian and Hookean elements (with $i=1, 2$), respectively.

In the frequency-domain, **Equation 1** writes as follows:

$$\widehat{\sigma}(\omega)(1 + \kappa_1 i\omega - \tau_1 \tau_3 \omega^2) = \widehat{\varepsilon}(\omega)(\eta_2 i\omega - \tau_1 \eta_2 \omega^2) \quad 2$$

where, $\widehat{\sigma}(\omega)$ and $\widehat{\varepsilon}(\omega)$ are the Fourier transforms (“ $\widehat{}$ ”) of the axial stress $\sigma(t)$ and strain $\varepsilon(t)$, respectively; whereas, $\tau_1 = \eta_1/E_1$, $\tau_2 = \eta_2/E_1$, $\tau_3 = \eta_2/E_2$, $\kappa_1 = (\tau_1 + \tau_2 + \tau_3)$, and i is the imaginary unit ($i^2 = -1$). **Equation 3** provides a means for evaluating the frequency-dependent compressional complex modulus:

$$E^*(\omega) = \frac{\widehat{\sigma}(\omega)}{\widehat{\varepsilon}(\omega)} = \frac{(\tau_2 + \tau_3 + \tau_1^2 \tau_3 \omega^2)}{(1 - \tau_1 \tau_3 \omega^2)^2 + (\kappa_1 \omega)^2} \eta_2 \omega^2 + i \frac{[1 + (\tau_1 + \tau_2) \tau_1 \omega^2]}{(1 - \tau_1 \tau_3 \omega^2)^2 + (\kappa_1 \omega)^2} \eta_2 \omega = E'(\omega) + i E''(\omega) \quad 3$$

which provides information on both the elastic (via the compressional storage modulus $E'(\omega)$) and the viscous (via the compressional loss modulus $E''(\omega)$) nature of the system under study.

In this work, we exploited **Equation 3** to evaluate the (non-linear) viscoelastic properties of spheroids either (i) by a regression of the experimental data in the time-domain (i.e., $\sigma(t)$, $\varepsilon(t)$) by means of **Equation 1** to determine the parameters η_1 , η_2 , E_1 and E_2 , or (ii) by a direct transformation of the stress & strain raw experimental data by means of i-Rheo [44], which is a model-free algorithm that allows the evaluation of the frequency-dependent complex modulus through the ratio of the Fourier transforms of the axial stress $\sigma(t)$ and strain $\varepsilon(t)$. A direct comparison of the outcomes of the two approaches above is presented hereafter.

2.5. Rheological setup

Conventional oscillatory bulk-rheology measurements of the hydrogels were performed by using a stress-controlled rheometer (Anton Paar Physica MCR 302 Instrument) equipped with a parallel plate measuring system of 25mm diameter (PP25-SN36246). Mechanical properties were investigated by means of strain (γ) sweep tests, spanning from 0.01% to 1% at an angular frequency (ω) of 10 rads^{-1} . Measurements were performed on dry hydrogels samples of cylindrical shape, without the addition of water to their edges to avoid swelling. The samples had a diameter of 29.1 mm and an initial thickness of 1.5 mm \pm 0.1 mm. The frequency-dependent materials' linear viscoelastic properties were represented by their shear complex modulus: $G^*(\omega) = G'(\omega) + iG''(\omega)$; which is a complex

number whose real and imaginary parts provide information on the elastic and viscous nature of the material under investigation.

2.6. Nanoindenter

The effectiveness of the proposed method has been further corroborated by means of measurements performed with a nanoindenter device, referred as Chiaro (Optics11, Netherlands) [58], mounted on top of an inverted phase contrast microscope (Evos XL Core, Thermofisher, UK). All measurements were performed with the same cantilever having a stiffness $k = 0.026$ N/m and a spherical tip of 46 μm diameter. For each sample, measurements were repeated in at least 3 different spots.

To conduct these measurements, hydrogel samples with a cylindrical shape having a radius of 17 mm and an initial thickness of $1.5 \text{ mm} \pm 0.1 \text{ mm}$ were positioned in a petri dish filled with approximately 3 mL of distilled water.

Spheroids were picked using a pipette (preferably with a cut tip to avoid damage during loading) and were seeded in a petri dish previously filled with approximately 3 mL of standard growth medium, few hours before the experiment, allowing the spheroids to adhere to the petri dish but preserving their 3D structure.

The typical creep test was conducted through load control tests to replicate our rheo-optical test conditions. The shear storage and loss moduli at each frequency were calculated for both systems using the i-Rheo method [46, 59].

2.7. Hydrogels preparation

Hydrogels were synthesized through the crosslinking of polyacrylamide solutions, prepared either with Acrylamide/Bis Solution (40% Acrylamide/Bis Solution, 29:1, Bio-Rad, #1610147) or Acrylamide/Bis Crosslinker powder in a 10:1 ratio (Acrylamide, Bio-Rad, #1610100, and Bis Crosslinker, Bio-Rad, #1610200). The concentrations utilized spanned a range (5% to 15% v/v for Acrylamide/Bis Solution and 4% to 8% wt for Acrylamide/Bis Crosslinker powder) selected to yield

hydrogels exhibiting mechanical properties resembling those found in diverse biological tissues. This systematic variation in concentration allows for the tailoring of hydrogel properties to mimic the mechanical characteristics of a wide variety of tissues [60, 61], enhancing their versatility for applications in biomedical and scientific research.

For sample preparation, the requisite amount of polymer and crosslinker was homogeneously mixed with distilled water, yielding a final solution volume of 20 mL. Subsequently, 200 μ L of ammonium persulfate (APS) with a concentration of 10% w/v was introduced into the solution, initiating the polymerization reaction through the addition of 20 μ L of N,N,N',N'-Tetramethylethylenediamine accelerator (TEMED).

Hydrogel solutions, approximately 10 mL in volume, were cast between two glass plates separated by a spacer measuring 1.5 mm in thickness (Bio-Rad Mini-PROTEAN Spacer Plates with 1.5 mm Integrated Spacers, #1653312). Following polymerization, typically requiring approximately 30 minutes at room temperature, the glass plates were removed. The resulting gel structures were subsequently molded into cylindrical shapes resembling pills, possessing a thickness of $1.5 \text{ mm} \pm 0.1 \text{ mm}$. This molding process involved the use of a circular cutter to match the diameter of the rheometer tool, ensuring dimensions suitable for subsequent analysis with a nanoindenter.

2.8. Statistical analysis

Nanoindentation measurements were repeated at least in 3 different spots for biomimetic hydrogels and biological samples. At least 5 spheroids were analysed for each cell lines (tumoral and non-tumoral) for both nanoindenter and rheo-optical compression tests. Data are expressed as mean \pm standard error of mean (SEM).

3. Results

Rheo-optical compression tests were initially conducted on PANC-1 spheroids. To validate our technique, a similar creep test was performed by using a nanoindentation test on spheroids and,

subsequently, on two biomimetic hydrogels. Concerning the hydrogels, their viscoelastic properties were determined by applying i-Rheo to nanoindentation results, and these outcomes were then compared with those obtained through traditional oscillatory bulk-rheology measurements, as described below. After validating this methodology, we applied the i-Rheo-optical assay to a second cell line, NIH/3T3, which served as the non-tumoral control.

3.1. *i-Rheo-optical assay PANC-1 spheroids*

Constant-load creep tests were conducted on PANC-1 spheroids. In **Figure 2A** representative phase contrast microscopy images of PANC-1 tumoral spheroids are reported; each image refers to a different time measured from the start of the experiment. Preliminary visual analysis of these images reveals a significant expansion of the spheroids' cross-section perpendicular to the compressional force within the initial seconds of the experiment, swiftly attaining a relatively stable and uniform deformed state. In **Figure 2B**, the average value of stress ($\sigma(t)$), evaluated across at least 10 spheroids, is plotted as a function of time, t . Due to the constant-load compression, the spheroid's area increased over time, leading to a reduction in $\sigma(t)$ because of its definition as the ratio between the loading force and the contact area (see **2 section**). The resulting strain history, obtained through image analysis, is shown in **Figure 2C**. The number of experimental data points (circles) reported in **Figure 2B and C**, has been reduced to improve the readability of the outcomes. Experimental data were fitted by means of the Burgers model (i.e., **Equation 1**, solid blue line) to determine the coefficients η_1 , η_2 , E_1 and E_2 . These coefficients were subsequently utilized to calculate $E'(\omega)$ and $E''(\omega)$ via **Equation 3**, and the outcomes were compared with those obtained via creep measurements processed by means of i-Rheo, as shown in **Figure 2D**, from which a very good agreement between the two methods is apparent.

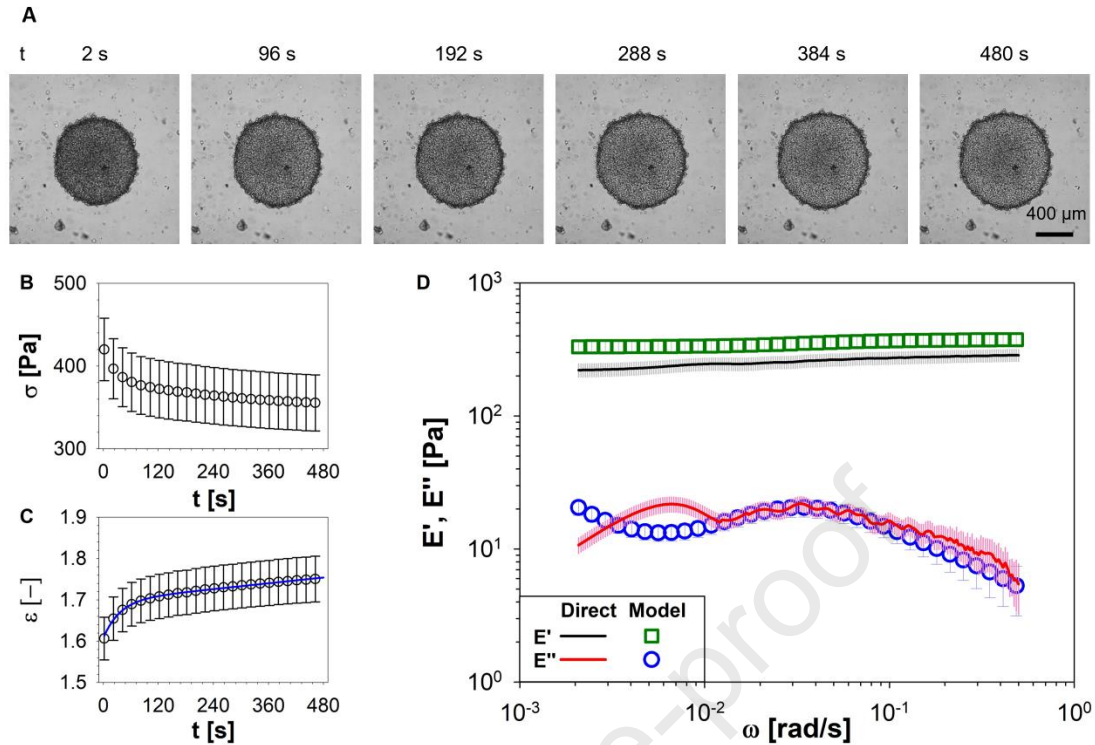


Figure 2. *i*-Rheo-optical compression assay performed on PANC-1 spheroids. **A)** Representative phase-contrast microscopy images showing the morphological response of PANC-1 spheroids at six different times: 2, 96, 192, 288, 384 and 480 s. Images of the panel are relative to a single spheroid, taken as a qualitative representation of a given experimental condition. Scale bar: 200 μm . **B)** Evolution of stress, $\sigma(t)$, defined as the ratio between constant loading force and the evolution of spheroid area. **C)** Morphological response of biological system in terms of strain, ϵ . Experimental data (circle symbols) were fitted by using Burgers model (i.e., Equation 1, solid blue line). **D)** Comparison between the viscoelastic compressional moduli obtained by using either the Burgers model in the frequency domain (i.e. Equation 3, open symbols) or the model-free *i*-Rheo, applied to the raw data from the compression assay (lines). Data were averaged on at least 10 spheroids.

3.2. Cross-Methodology Validation

3.2.1. *i*-Rheo-optical assay vs. Nanoindentation

Load control tests were conducted on PANC-1 spheroids using a nanoindenter to establish a comparative analysis with outcomes derived from two distinct methodologies: the rheo-optical compression assay and nanoindentation. In **Figure 3A** a representative phase contrast microscopy image of a PANC-1 spheroid is reported. Cellular spheroids were indented at fixed load, using the deflection of the cantilever (on the left in **Figure 3A**) as a measure of the displacement. The time-dependent relationship between load, $F(t)$, and displacement, $\delta(t)$, showed in **Figure 3B**, for each spheroid was assessed in the Fourier domain to quantify its linear viscoelastic properties, as shown in **Figure 3C**. The viscoelastic response demonstrated a good agreement between the two methodologies, not only in terms of the absolute values of the moduli but also in their behaviour

across the common angular frequency range. This consistency in results between the rheo-optical compression assay and nanoindentation further substantiates the effectiveness of the innovative technique for assessing viscoelastic properties in these biological samples.

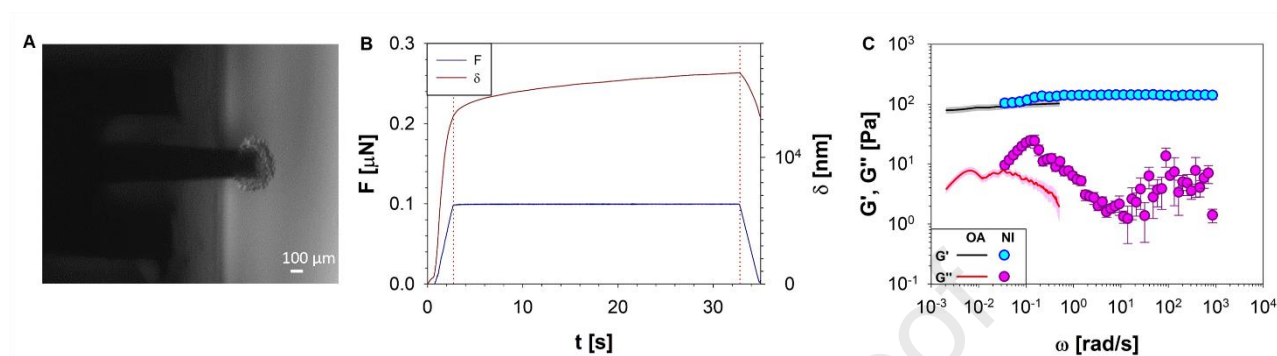


Figure 3. *A)* Representative phase-contrast microscopy images showing the PANC-1 spheroids indented with the cantilever on the left. Image is relative to a single spheroid, taken as a qualitative representation of a specific experimental condition. Scale bar: 100 μm. *B)* The time-dependent relationship between load, $F(t)$, and displacement, $\delta(t)$, for to a single spheroid. *C)* Comparison between the viscoelastic shear moduli of the spheroids measured by means of nanoindentation (symbols) and by the *i*-Rheo-optical compression approach (lines), with the outputs divided by 2.8 to account for the relationship between compressional and shear moduli: $E=2G(1+\nu)$, where ν is the Poisson ratio, assumed to be 0.4 [62] for both the sets of measurements. However, it is important to note that maintaining the assumption of incompressibility, as outlined in Section 2.3 (i.e. $\nu=0.5$), would result in a decrease in the moduli by approximately 6.6%.

3.2.2. Nanoindentation vs. Bulk-Rheology

To further validate the methodologies presented in this work, load control indentations were also performed on two different polyacrylamide hydrogels, solution- and powder- based. Multiple measurements (≥ 10) were repeated at different gels concentrations. A comparison between the samples viscoelastic moduli measured by using a conventional bulk-rheology rheometer (filled symbols) and nanoindenter (open symbols) are reported (i) in **Figure 4** for solution-based hydrogels at concentrations of 5, 7, 10 and 15% v/v (**A**, **B**, **C**, and **D**, respectively) and (ii) in **Figure 5** for powder-based hydrogels at concentrations of 4, 6 and 8% wt (**A**, **B** and **C**, respectively). It is important to notice that the agreement between the two methods for G' values is better than that of G'' . This could be related to the fact that the analytical method used to analyse Nanoindentation measurements are based on the Hertz model, which was primarily developed for describing the deformation of purely elastic solid, thus neglecting their viscous behaviour. Additionally, the correlation between

$\sigma(t)-\varepsilon(t)$ is approximated to a first-order relation, which does not allow for a more precise evaluation of the Young's modulus.

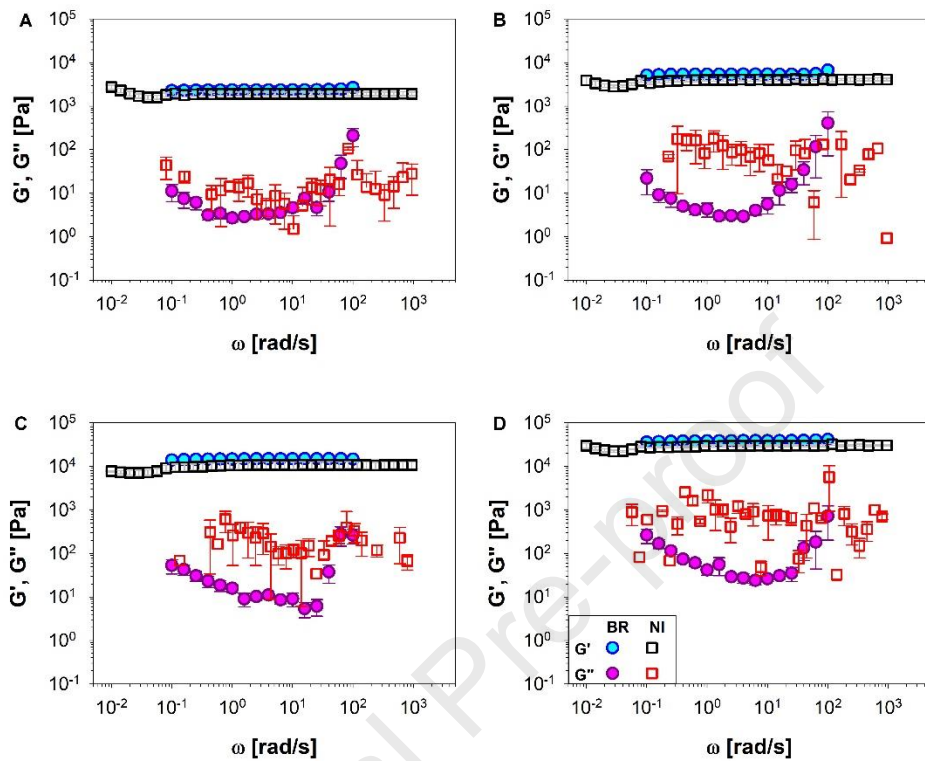


Figure 4. The shear storage modulus, G' , and the shear loss modulus, G'' , versus the angular frequency, ω , measured by means of a conventional bulk-rheology rheometer (blue and purple circle symbols) and by means of a nanoindenter (black and red square symbols) for polyacrylamide solution-based hydrogel at different concentrations: 5, 7, 10 and 15% v/v (A, B, C, and D, respectively).

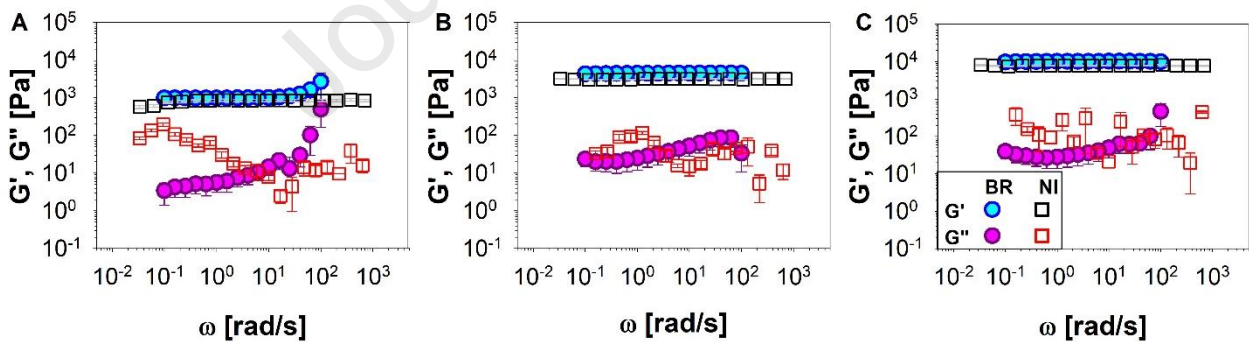


Figure 5. The shear storage modulus, G' , and the shear loss modulus, G'' , versus the angular frequency, ω , measured by means of a conventional bulk-rheology rheometer (blue and purple circle symbols) and by means of a nanoindenter (black and red square symbols) for polyacrylamide powder-based hydrogel at different concentrations: 4, 6 and 8% wt (A, B, and C, respectively).

3.3. *i*-Rheo-optical assay NIH/3T3 spheroids

For NIH/3T3 cells, illustrative phase contrast microscopy images showing non-tumoral spheroids at different timestamps are presented in **Figure 6A**. At a glance, it can be seen that the spheroids primarily expanded during the initial phase of the experiment under the influence of compressive

stress. Subsequently, they reach a relatively stable and consistent deformed state. In **Figure 6B** and **C**, the average stress values and the corresponding strain history are plotted against time, respectively. Also in this case, the duration of the whole experiment was 8 minutes, with an image acquisition rate of 0.5Hz. For clarity of the plot, not all the experimental data have been reported in the graph. The fitting parameters η_1 , η_2 , E_1 and E_2 were used to calculate the viscoelastic moduli via **Equation 3** and these were compared with those obtained by means of i-Rheo in **Figure 6D**. Notably, the results demonstrate a good agreement between the two methods, with a value of E' of circa $5.15 \cdot 10^2$ Pa and $3.46 \cdot 10^2$ Pa from the model and the direct evaluation, respectively, at ω approximately $2 \cdot 10^{-3}$ rad/s. By assuming a Poisson ratio, ν , of 0.4, G' is calculated to be $1.83 \cdot 10^2$ Pa and $1.23 \cdot 10^2$ Pa, respectively. These values are slightly higher than those of single cells from the same cell line (100 ± 10 Pa [63]), potentially attributed to the cell-cell and cell-ECM interactions.

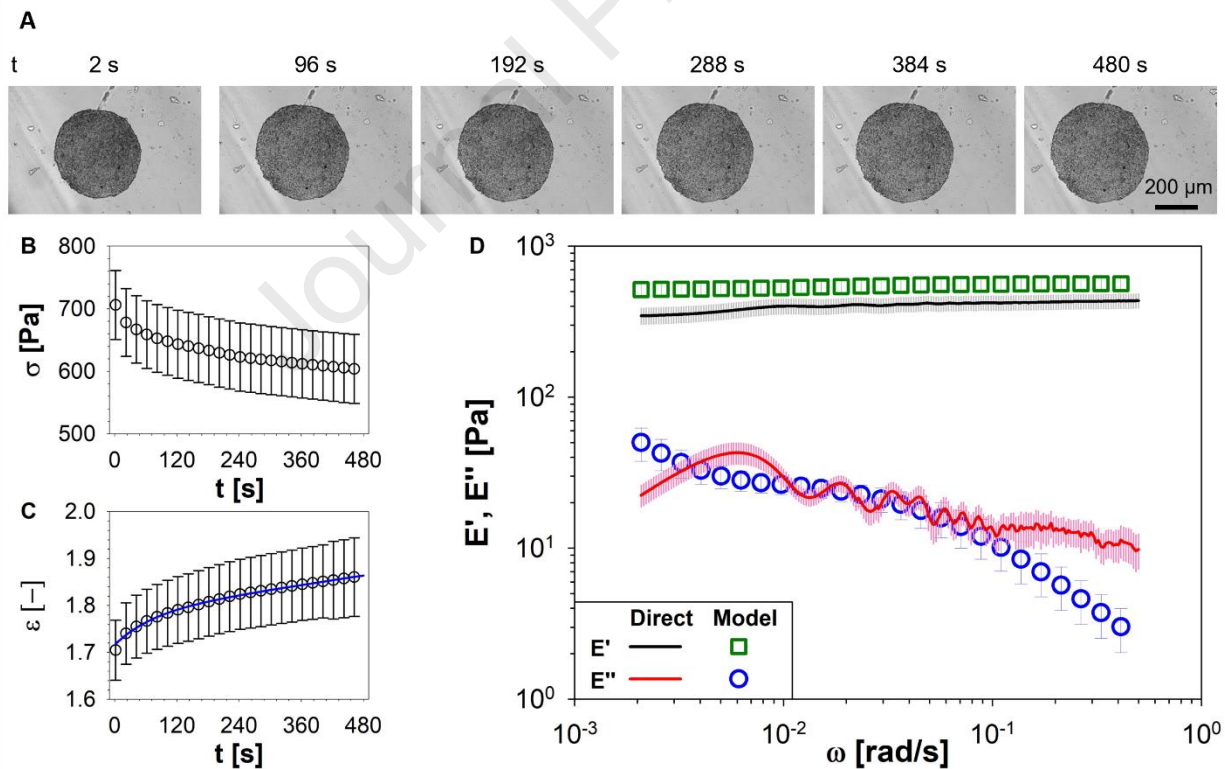


Figure 6. *i*-Rheo-optical compression assay performed on NIH/3T3 spheroids. **A)** Representative phase-contrast microscopy images showing the morphological response of NIH/3T3 spheroids at six different times: 2, 96, 192, 288, 384 and 480 s. Images of the panel are relative to a single spheroid, taken as a qualitative representation of a given experimental condition. Scale bar: 200 μ m. **B)** Evolution of stress, $\sigma(t)$, defined as the ratio between constant loading force and the evolution of spheroid contact area. **C)** Morphological response of biological system in terms of strain, ϵ . Experimental data (circle symbols) were fitted by using Burgers model (solid blue line). **D)** Comparison between the viscoelastic compressional moduli of the spheroids obtained either by using Burgers model in the frequency domain (i.e., Equation 3, open symbols) or by means of the model-free *i*-Rheo algorithm, applied to the raw data from the compression assay (lines). Data were averaged on at least 10 spheroids.

Across the analysed range of frequencies, both PANC-1 and NIH/3T3 cell lines exhibited frequency-dependent behaviours in their compressional storage, $E'(\omega)$, and compressional loss, $E''(\omega)$, moduli (refer to **Figure 2D** for PANC-1 and **Figure 6D** for NIH/3T3). A clear disparity in cellular elasticity is apparent between normal and tumoral cells, with PANC-1 cells being approximately 58.8% softer than normal NIH/3T3 ones, when compared in terms of their compressional elastic modulus $E'(\omega)$; an outcome that aligns well with other findings reported in literature [64]. Similarly, when comparing their viscous components, PANC-1 cells are found to be roughly 50% less viscous than NIH/3T3 spheroids.

For a clearer comparison between the i-Rheo and Burger model, data derived from the model-free approach were fitted with **Equation 3** to get the same parameter: η_1 , E_1 and τ_2 , where τ_2 is defined as η_2/E_2 . Both viscous and elastic components were summarized in **Figure 7**, for both cell lines using both approaches, with data from the Burger model plotted in red and data from i-Rheo in yellow.

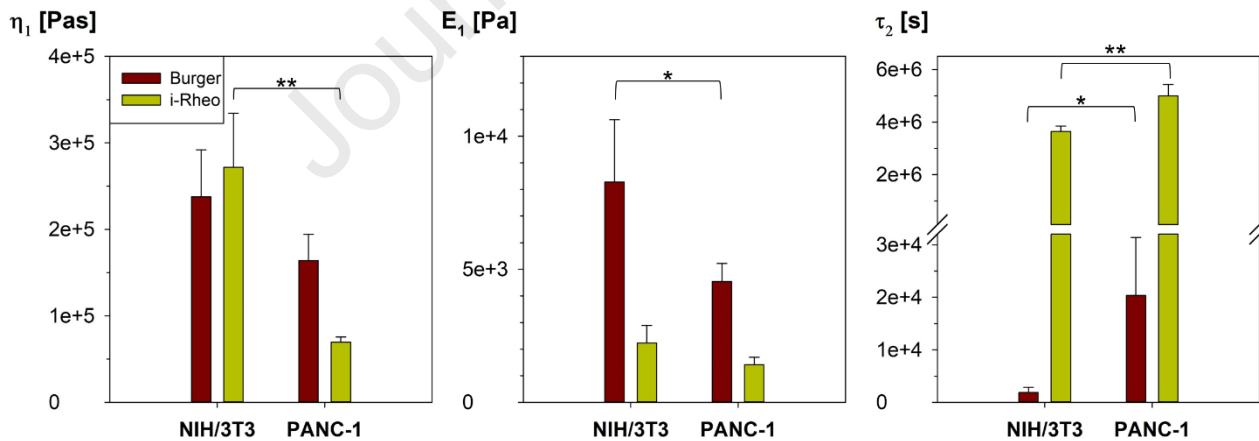


Figure 7. A comparison between the parameters of the Burgers model η_1 , E_1 and τ_2 , which is defined as the ratio between η_2 and E_2 , obtained either (i) by fitting Equation 1 to the compression data and then used them to calculate the viscoelastic moduli via Equation 3 for both NIH/3T3 and PANC-1 cell lines (represented in red); or (ii) by fitting the outcomes obtained from the model-free i-Rheo method by using directly Equation 3 for both cell lines (represented in yellow). Statistical significance of the results: * $p < 0.05$ and ** $p < 0.005$ versus control cells.

As shown in **Figure 7**, the analysis of the parameters of the Burgers model E_1 , η_1 and τ_2 , could serve as possible indicators for discriminating between spheroids based on their viscoelastic properties. In

particular, E_1 represents the instantaneous response, while η_1 is associated with long-term viscous flow. Conversely, η_2 and E_2 are ‘linked’ to the retarded elastic behaviour, characterizing the middle section of the response curve. According to **Figure 7** and consistent with literature [65], the η_1 value of non-tumoral spheroids (0.267 ± 0.052 MPa·s) is higher than that of tumoral spheroids (0.164 ± 0.030 MPa·s). This observation aligns with previous findings suggesting that at a fixed viscosity of the surrounding ECM, a lower viscous cell generates a more pronounced fingering pattern at the interface [26]. Consequently, this parameter may be used to estimate the level of invasion and the metastatic process. Similarly, tumoral spheroids exhibit a lower elastic modulus compared to non-tumoral ones, in agreement with prior research [66]. This observation confirms the critical role of the elastic modulus in understanding the cell’s ability to invade blood vessels, which is influenced by their deformability. Ultimately, τ_2 , defined as the ratio between η_2 and E_2 , emerges as the sole parameter among the three investigated capable of distinguishing between the two cell lines for both analytical approaches explored in this paper. Notably, upon comparing the statistical significance of the results shown in Figure 7, the model-free i-Rheo assay yields a higher level of confidence in distinguishing between the two cell lines.

Interestingly, **Figure 8** reveals that in the lower range of the explored frequencies, the non-tumoral NIH/3T3 cells exhibit a higher loss tangent value, $\tan(\delta) = E''(\omega)/E'(\omega)$, than the cancerous PANC-1 cells, consistently across both i-Rheo-optical assay (lines) and Burgers (symbols) analytical methods. This observation is consistent with the intrinsic characteristics of fibroblasts, whose higher degree of elasticity can be attributed to their distinctive morphology and elevated extracellular matrix (ECM) production in comparison to epithelial cells [67]. In contrast, the cancerous PANC-1 cells exhibit a higher value of $\tan(\delta)$ at relatively high frequencies (i.e., $\omega > 10^{-2}$ rad/s), reflecting their greater deformability when compared to non-tumoral NIH/3T3 cells; an attribute that is congruent with their invasive and migratory capabilities.

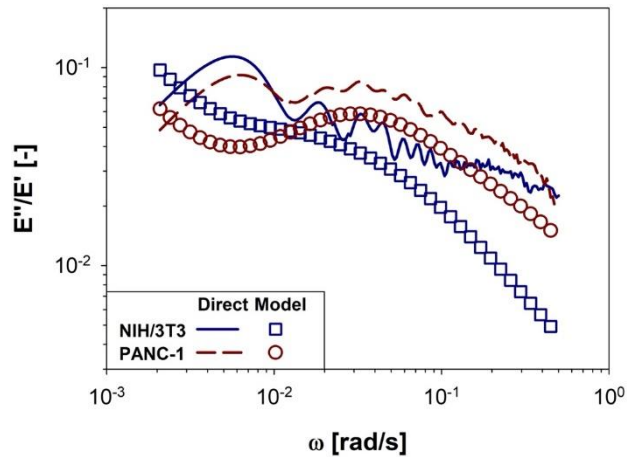


Figure 8. Comparison between the loss tangent, $E''(\omega)/E'(\omega)$, as a function of angular frequency, ω , for both cell lines NIH/3T3 (open squares and continuous line) and PANC-1 (open circles and dashed line). The data have been obtained by using either the Burgers model in the frequency domain (i.e. Equation 3, open symbols) or the model-free *i*-Rheo, applied to the raw data from the compression assay (lines).

Conclusion

This study introduces a new ‘*i*-Rheo-optical assay’ that integrates rheology with optical microscopy to analyse the viscoelastic properties of multicellular spheroids. Representing a notable advancement in biophysical research, the assay bridges a critical knowledge gap in understanding the viscoelastic nature of multicellular systems, an area traditionally limited to measuring the elastic modulus. Utilizing a straightforward and cost-effective approach with microscope glass coverslips as the applied load to cell spheroids in standard cell culture plates, this assay was first validated by using PANC-1 tumoral spheroids and subsequently applied to non-tumoral NIH/3T3 spheroids. The strength of our approach lies in its capacity to provide comprehensive viscoelastic moduli data, encompassing both surface cells of spheroids and their interaction with internal spheroid structure and ECM accumulation [68]. This differs from other sophisticated and costly instruments such as AFM or Nanoindenter, which primarily approximate biological samples as purely elastic tissues by using the Hertz model and utilize micrometric tips, thus limiting the investigations to very small regions and neglecting heterogeneities present in both biological samples and hydrogels [69].

By leveraging the open-access, model-free tool i-Rheo, we derived their frequency-dependent viscoelastic moduli through Fourier transforms of their time-dependent stress/strain curves, with results aligning well with predictions from the Burgers model. Further validation through (i) nanoindentation tests on PANC-1 spheroids and (ii) conventional oscillatory bulk-rheology measurements on biomimetic hydrogels, corroborated the general validity of the novel assay.

The results demonstrate the potential of i-Rheo-optical assay by revealing distinct frequency-dependent viscoelastic moduli values for different cell lines, opening avenues for identifying effective biomarkers critical in discriminating healthy tissues from pathological equivalents. Furthermore, although we assumed a Poisson ratio of 0.4 based on literature, our i-Rheo-optical assay has the capability to deducing the correct ν by collapsing E' and G' [70].

Beyond laboratory applications, the assay's adaptability and scalability make it potentially useful in various biophysical contexts, enriching our understanding of cellular mechanics in diverse biological systems, including biopsies. Moving forward, our future investigations aim to compare different cell types originating from the same tissue, such as breast tissue, with the goal of quantifying variations in elastic and viscous moduli between non-tumoral cells (e.g., MCF-10a) and tumoral ones, while also discerning differences in invasion potential and metastatic capacity (e.g., MCF7 and MBA-MD-231). Additionally, we seek to explore the influence of ECM generated during spheroid formation, as it may impact distinct properties [25] contingent upon the amount of ECM produced and the resulting maturation of spheroids, including the duration of post-preparation incubation. Furthermore, within the realm of biopsies, we aim to quantify the effects of gender (male and female), age, and health status on tissue viscoelastic properties.

This innovation promises significant contributions to tissue engineering, cancer research, and therapeutic development, offering new insights into the study of cellular and tissue mechanics.

Author Contributions

Rosalia Ferraro: Data curation (main); Formal analysis (equal); Investigation (main); Methodology (equal); Software (equal); Validation (equal); Writing – original draft (equal); Writing – review & editing (equal). Stefano Guido: Methodology (equal); Supervision (equal); Writing – original draft (equal); Writing – review & editing (equal). Sergio Caserta: Conceptualization (equal); Data curation (equal); Formal analysis (equal); Funding acquisition (equal); Investigation (equal); Methodology (equal); Project administration (equal); Supervision (equal); Validation (equal); Writing – original draft (equal); Writing – review & editing (equal). Manlio Tassieri: Conceptualization (equal); Data curation (equal); Formal analysis (equal); Funding acquisition (equal); Investigation (equal); Methodology (equal); Project administration (equal); Supervision (equal); Validation (equal); Writing – original draft (equal); Writing – review & editing (equal).

Informed Consent Statement

Informed consent was waived for this study, as it involved the use of immortalized cell lines obtained from the American Type Culture Collection (ATCC, Manassas, VA).

Acknowledges

M.T. and R.F. acknowledge support from the Technology Touching Life initiative through an EPSRC/BBSRC/MRC joint grant “Experiencing the micro-world—a cell’s perspective” (EP/R035067/1, EP/R035563/1, and EP/R035156/1) <http://nu-sense.ac.uk/home.aspx>. R.F. acknowledges the contribution of Vincenzo Pepe to the experiments, data analysis, and data interpretation, as part of his master's thesis. We thank Renata Cia Sanches Loberto for drawing the graphical abstract. We are grateful to the three anonymous reviewers for their invaluable and constructive criticisms, which have enhanced the quality of the manuscript.

References

- [1] R.C. Boot, G.H. Koenderink, P.E. Boukany, Spheroid mechanics and implications for cell invasion, *Advances in Physics: X* 6(1) (2021) 1978316. <https://doi.org/10.1080/23746149.2021.1978316>
- [2] D.C. Vuoso, S. D'Angelo, R. Ferraro, S. Caserta, S. Guido, M. Cammarota, M. Porcelli, G. Cacciapuoti, Annurca apple polyphenol extract promotes mesenchymal-to-epithelial transition and inhibits migration in triple-negative breast cancer cells through ROS/JNK signaling, *Scientific reports* 10(1) (2020) 1-17. <https://doi.org/10.1038/s41598-020-73092-2>
- [3] F. Ascione, S. Caserta, S. Guido, The wound healing assay revisited: A transport phenomena approach, *Chemical Engineering Science* 160 (2017) 200-209. <https://doi.org/10.1016/j.ces.2016.11.014>
- [4] Y. Harada, Y. Tanaka, M. Terasawa, M. Pieczyk, K. Habiro, T. Katakai, K. Hanawa-Suetsugu, M. Kukimoto-Niino, T. Nishizaki, M. Shirouzu, DOCK8 is a Cdc42 activator critical for interstitial dendritic cell migration during immune responses, *Blood, The Journal of the American Society of Hematology* 119(19) (2012) 4451-4461. <https://doi.org/10.1182/blood-2012-01-407098>
- [5] A.A.L. Baeyens, S.R. Schwab, Finding a way out: S1P signaling and immune cell migration, *Annual Review of Immunology* 38 (2020) 759-784. <https://doi.org/10.1146/annurev-immunol-081519-083952>
- [6] Y. Ding, J. Xu, J.S. Bromberg, Regulatory T cell migration during an immune response, *Trends in immunology* 33(4) (2012) 174-180. <https://doi.org/10.1016/j.it.2012.01.002>
- [7] P. Gassmann, J. Haier, The tumor cell–host organ interface in the early onset of metastatic organ colonisation, *Clinical & experimental metastasis* 25(2) (2008) 171-181. <https://doi.org/10.1007/s10585-007-9130-6>
- [8] A.B. Mariotto, R. Etzioni, M. Hurlbert, L. Penberthy, M. Mayer, Estimation of the number of women living with metastatic breast cancer in the United States, *Cancer Epidemiology, Biomarkers & Prevention* 26(6) (2017) 809-815. <https://doi.org/10.1158/1055-9965.EPI-16-0889>
- [9] Q.T. Ostrom, C.H. Wright, J.S. Barnholtz-Sloan, Brain metastases: epidemiology, *Handbook of clinical neurology* 149 (2018) 27-42. <https://doi.org/10.1016/B978-0-12-811161-1.00002-5>
- [10] J. Hoarau-Véchet, A. Rafii, C. Touboul, J. Pasquier, Halfway between 2D and animal models: are 3D cultures the ideal tool to study cancer-microenvironment interactions?, *International journal of molecular sciences* 19(1) (2018) 181. <https://doi.org/10.3390/ijms19010181>
- [11] Y.M. Efremov, I.M. Zurina, V.S. Presniakova, N.V. Kosheleva, D.V. Butnaru, A.A. Svistunov, Y.A. Rochev, P.S. Timashev, Mechanical properties of cell sheets and spheroids: the link between single cells and complex tissues, *Biophysical Reviews* 13(4) (2021) 541-561. <https://doi.org/10.1007/s12551-021-00821-w>
- [12] G. Mehta, A.Y. Hsiao, M. Ingram, G.D. Luker, S. Takayama, Opportunities and challenges for use of tumor spheroids as models to test drug delivery and efficacy, *Journal of controlled release* 164(2) (2012) 192-204. <https://doi.org/10.1016/j.jconrel.2012.04.045>
- [13] T. Rodrigues, B. Kundu, J. Silva-Correia, S.C. Kundu, J.M. Oliveira, R.L. Reis, V.M. Correlo, Emerging tumor spheroids technologies for 3D in vitro cancer modeling, *Pharmacology & therapeutics* 184 (2018) 201-211. <https://doi.org/10.1016/j.pharmthera.2017.10.018>
- [14] F. Hirschhaeuser, H. Menne, C. Dittfeld, J. West, W. Mueller-Klieser, L.A. Kunz-Schughart, Multicellular tumor spheroids: an underestimated tool is catching up again, *Journal of biotechnology* 148(1) (2010) 3-15. <https://doi.org/10.1016/j.jbiotec.2010.01.012>
- [15] M.W. Laschke, M.D. Menger, Spheroids as vascularization units: From angiogenesis research to tissue engineering applications, *Biotechnology advances* 35(6) (2017) 782-791. <https://doi.org/10.1016/j.biotechadv.2017.07.002>

- [16] E.C. Costa, A.F. Moreira, D. de Melo-Diogo, V.M. Gaspar, M.P. Carvalho, I.J. Correia, 3D tumor spheroids: an overview on the tools and techniques used for their analysis, *Biotechnology advances* 34(8) (2016) 1427-1441. <https://doi.org/10.1016/j.biotechadv.2016.11.002>
- [17] M. Chatzinikolaïdou, Cell spheroids: the new frontiers in in vitro models for cancer drug validation, *Drug Discovery Today* 21(9) (2016) 1553-1560. <https://doi.org/10.1016/j.drudis.2016.06.024>
- [18] S.J. Kim, E.M. Kim, M. Yamamoto, H. Park, H. Shin, Engineering Multi-Cellular Spheroids for Tissue Engineering and Regenerative Medicine, *Advanced Healthcare Materials* 9(23) (2020). <https://doi.org/10.1002/adhm.202000608>.
- [19] A.S. Nunes, A.S. Barros, E.C. Costa, A.F. Moreira, I.J. Correia, 3D tumor spheroids as in vitro models to mimic in vivo human solid tumors resistance to therapeutic drugs, *Biotechnology and bioengineering* 116(1) (2019) 206-226. <https://doi.org/10.1002/bit.26845>
- [20] M. Kapałczyńska, T. Kolenda, W. Przybyła, M. Zajączkowska, A. Teresiak, V. Filas, M. Ibbs, R. Bliźniak, Ł. Łuczewski, K. Lamperska, 2D and 3D cell cultures—a comparison of different types of cancer cell cultures, *Archives of medical science: AMS* 14(4) (2018) 910. <https://doi.org/10.5114/aoms.2016.63743>
- [21] A. Nyga, U. Cheema, M. Loizidou, 3D tumour models: novel in vitro approaches to cancer studies, *Journal of cell communication and signaling* 5(3) (2011) 239-248. <https://doi.org/10.1007/s12079-011-0132-4>
- [22] K.M. Yamada, E. Cukierman, Modeling tissue morphogenesis and cancer in 3D, *Cell* 130(4) (2007) 601-610. <https://doi.org/10.1016/j.cell.2007.08.006>
- [23] J.L. Horning, S.K. Sahoo, S. Vijayaraghavalu, S. Dimitrijevic, J.K. Vasir, T.K. Jain, A.K. Panda, V. Labhassetwar, 3-D tumor model for in vitro evaluation of anticancer drugs, *Molecular pharmaceutics* 5(5) (2008) 849-862. <https://doi.org/10.1021/mp800047v>
- [24] P. Marmottant, A. Mgharbel, J. Käfer, B. Audren, J.-P. Rieu, J.-C. Vial, B. Van Der Sanden, A.F.M. Marée, F. Graner, H. Delanoë-Ayari, The role of fluctuations and stress on the effective viscosity of cell aggregates, *Proceedings of the National Academy of Sciences* 106(41) (2009) 17271-17275. <https://doi.org/10.1073/pnas.0902085106>
- [25] D. Tsvirkun, J. Revilloud, A. Giannetti, C. Verdier, The intriguing role of collagen on the rheology of cancer cell spheroids, *Journal of Biomechanics* 141 (2022). <https://doi.org/10.1016/j.jbiomech.2022.111229>.
- [26] A. Elosegui-Artola, The extracellular matrix viscoelasticity as a regulator of cell and tissue dynamics, *Current opinion in cell biology* 72 (2021) 10-18. <https://doi.org/10.1016/j.ccb.2021.04.002>
- [27] L. Andolfi, S.L.M. Greco, D. Tierno, R. Chignola, M. Martinelli, E. Giolo, S. Luppi, I. Delfino, M. Zanetti, A. Battistella, Planar AFM macro-probes to study the biomechanical properties of large cells and 3D cell spheroids, *Acta Biomaterialia* 94 (2019) 505-513. <https://doi.org/10.1016/j.actbio.2019.05.07>
- [28] S. Sakuma, A. Sato, N. Kojima, F. Tao, F. Arai, Force sensor probe using quartz crystal resonator with wide measurement range for mechanical characterization of HepG2 spheroid, *Sensors and Actuators A: Physical* 265 (2017) 202-210. <https://doi.org/10.1016/j.sna.2017.08.033>
- [29] H. Liu, J. Wen, Y. Xiao, J. Liu, S. Hopyan, M. Radisic, C.A. Simmons, Y. Sun, In situ mechanical characterization of the cell nucleus by atomic force microscopy, *ACS nano* 8(4) (2014) 3821-3828. <https://doi.org/10.1021/nn500553z>
- [30] Y. Abidine, A. Giannetti, J. Revilloud, V.M. Laurent, C. Verdier, Viscoelastic Properties in Cancer: From Cells to Spheroids, *Cells* 10(7) (2021). <https://doi.org/10.3390/cells10071704>.
- [31] D. Jaiswal, N. Cowley, Z.C. Bian, G.A. Zheng, K.P. Claffey, K. Hoshino, Stiffness analysis of 3D spheroids using microweavers, *Plos One* 12(11) (2017). <https://doi.org/10.1371/journal.pone.0188346>.
- [32] K. Ito, S. Sakuma, M. Kimura, T. Takebe, M. Kaneko, F. Arai, Temporal transition of mechanical characteristics of HUVEC/MSK spheroids using a microfluidic chip with force sensor probes, *Micromachines* 7(12) (2016) 221. <https://doi.org/10.3390/mi7120221>

- [33] H.W. Hou, Q.S. Li, G.Y.H. Lee, A.P. Kumar, C.N. Ong, C.T. Lim, Deformability study of breast cancer cells using microfluidics, *Biomedical microdevices* 11(3) (2009) 557-564. <https://doi.org/10.1007/s10544-008-9262-8>
- [34] Q. Guo, S.M. McFaul, H. Ma, Deterministic microfluidic ratchet based on the deformation of individual cells, *Physical Review E* 83(5) (2011) 051910. <https://doi.org/10.1103/PhysRevE.83.051910>
- [35] L.Z. Yanez, J. Han, B.B. Behr, R.A.R. Pera, D.B. Camarillo, Human oocyte developmental potential is predicted by mechanical properties within hours after fertilization, *Nature communications* 7(1) (2016) 1-12. <https://doi.org/10.1038/ncomms10809>
- [36] A. Blumlein, N. Williams, J.J. McManus, The mechanical properties of individual cell spheroids, *Scientific Reports* 7 (2017) 10. <https://doi.org/10.1038/s41598-017-07813-5>.
- [37] M. Dolega, G. Zurlo, M. Le Goff, M. Greda, C. Verdier, J.F. Joanny, G. Cappello, P. Recho, Mechanical behavior of multi-cellular spheroids under osmotic compression, *Journal of the Mechanics and Physics of Solids* 147 (2021) 104205. <https://doi.org/10.1016/j.jmps.2020.104205>
- [38] A.P. Tabatabai, D.L. Kaplan, D.L. Blair, Rheology of reconstituted silk fibroin protein gels: the epitome of extreme mechanics, *Soft Matter* 11(4) (2015) 756-761. <https://doi.org/10.1039/C4SM02079K>
- [39] T.-M. Achilli, J. Meyer, J.R. Morgan, Advances in the formation, use and understanding of multi-cellular spheroids, *Expert opinion on biological therapy* 12(10) (2012) 1347-1360. <https://doi.org/10.1517/14712598.2012.707181>
- [40] E.C. Costa, D. de Melo - Diogo, A.F. Moreira, M.P. Carvalho, I.J. Correia, Spheroids formation on non - adhesive surfaces by liquid overlay technique: Considerations and practical approaches, *Biotechnology journal* 13(1) (2018) 1700417. <https://doi.org/10.1002/biot.201700417>
- [41] R. Ferraro, S. Caserta, S. Guido, A Low-Cost, User-Friendly Rheo-Optical Compression Assay to Measure Mechanical Properties of Cell Spheroids in Standard Cell Culture Plates, *Advanced Materials Technologies* n/a(n/a) (2024) 2301890. <https://doi.org/https://doi.org/10.1002/admt.202301890>.
- [42] O. Wintner, N. Hirsch - Attas, M. Schlossberg, F. Brofman, R. Friedman, M. Kupervaser, D. Kitsberg, A. Buxboim, A unified linear viscoelastic model of the cell nucleus defines the mechanical contributions of lamins and chromatin, *Advanced Science* 7(8) (2020) 1901222. <https://doi.org/10.1002/advs.201901222>
- [43] S. Tong, N.K. Singh, R. Sknepnek, A. Košmrlj, Linear viscoelastic properties of the vertex model for epithelial tissues, *PLoS computational biology* 18(5) (2022) e1010135. <https://doi.org/10.1371/journal.pcbi.1010135>
- [44] M. Tassieri, M. Laurati, D.J. Curtis, D.W. Auhl, S. Coppola, A. Scalfati, K. Hawkins, P.R. Williams, J.M. Cooper, i-Rheo: Measuring the materials' linear viscoelastic properties "in a step"!, *Journal of Rheology* 60(4) (2016) 649-660. <https://doi.org/10.1122/1.4953443>
- [45] R. Rivas-Barbosa, M.A. Escobedo-Sánchez, M. Tassieri, M. Laurati, i-Rheo: determining the linear viscoelastic moduli of colloidal dispersions from step-stress measurements, *Physical Chemistry Chemical Physics* 22(7) (2020) 3839-3848. <https://doi.org/10.1039/C9CP06191F>
- [46] Y.H. Chim, L.M. Mason, N. Rath, M.F. Olson, M. Tassieri, H. Yin, A one-step procedure to probe the viscoelastic properties of cells by Atomic Force Microscopy, *Scientific reports* 8(1) (2018) 1-12. <https://doi.org/10.1038/s41598-018-32704-8>
- [47] R. Leek, D.R. Grimes, A.L. Harris, A. McIntyre, Methods: using three-dimensional culture (spheroids) as an in vitro model of tumour hypoxia, *Tumor microenvironment*, Springer2016, pp. 167-196. https://doi.org/10.1007/978-3-319-26666-4_10
- [48] K. Aizel, A.G. Clark, A. Simon, S. Geraldo, A. Funfak, P. Vargas, J. Bibette, D.M. Vignjevic, N. Bremond, A tuneable microfluidic system for long duration chemotaxis experiments in a 3D collagen matrix, *Lab on a Chip* 17(22) (2017) 3851-3861. <https://doi.org/10.1039/C7LC00649G>

- [49] R. Ferraro, F. Ascione, P. Dogra, V. Cristini, S. Guido, S. Caserta, Diffusion-induced anisotropic cancer invasion: a novel experimental method based on tumour spheroids, *AIChE Journal* n/a(n/a) e17658. <https://doi.org/https://doi.org/10.1002/aic.17678>.
- [50] W.N. Findley, F.A. Davis, *Creep and relaxation of nonlinear viscoelastic materials*, Courier corporation 2013.
- [51] Y. Meng, Y. Xia, T.M. Young, Z. Cai, S. Wang, Viscoelasticity of wood cell walls with different moisture content as measured by nanoindentation, *RSC Advances* 5(59) (2015) 47538-47547. <https://doi.org/10.1039/C5RA05822H>
- [52] S.-F. Chuang, S.-Y. Lin, P.-J. Wei, C.-F. Han, J.-F. Lin, H.-C. Chang, Characterization of the elastic and viscoelastic properties of dentin by a nanoindentation creep test, *Journal of biomechanics* 48(10) (2015) 2155-2161. <https://doi.org/10.1016/j.jbiomech.2015.01.034>
- [53] D. Wang, L. Lin, F. Fu, The difference of creep compliance for wood cell wall CML and secondary S2 layer by nanoindentation, *Mechanics of Time-Dependent Materials* 25(2) (2021) 219-230. <https://doi.org/10.1007/s11043-019-09436-x>
- [54] T.N. Shepherd, J. Zhang, T.C. Ovaert, R.K. Roeder, G.L. Niebur, Direct comparison of nanoindentation and macroscopic measurements of bone viscoelasticity, *Journal of the mechanical behavior of biomedical materials* 4(8) (2011) 2055-2062. <https://doi.org/10.1016/j.jmbbm.2011.07.004>
- [55] X. Hong, J.P. Stegemann, C.X. Deng, Microscale characterization of the viscoelastic properties of hydrogel biomaterials using dual-mode ultrasound elastography, *Biomaterials* 88 (2016) 12-24. <https://doi.org/10.1016/j.biomaterials.2016.02.019>
- [56] N. Madani, A. Mojra, Quantitative diagnosis of breast tumors by characterization of viscoelastic behavior of healthy breast tissue, *Journal of the mechanical behavior of biomedical materials* 68 (2017) 180-187. <https://doi.org/10.1016/j.jmbbm.2017.01.044>
- [57] M. Osika, P. Kijanka, Ultrasound Shear Wave Propagation Modeling in General Tissue-Like Viscoelastic Materials, *Ultrasound in Medicine & Biology* 50(4) (2024) 627-638. <https://doi.org/10.1016/j.ultrasmedbio.2024.01.008>
- [58] A. Bartolozzi, F. Viti, S. De Stefano, F. Sbrana, L. Petecchia, P. Gavazzo, M. Vassalli, Development of label-free biophysical markers in osteogenic maturation, *Journal of the Mechanical Behavior of Biomedical Materials* 103 (2020) 103581. <https://doi.org/10.1016/j.jmbbm.2019.103581>
- [59] J.A. Moreno - Guerra, I.C. Romero - Sánchez, A. Martínez - Borquez, M. Tassieri, E. Stiakakis, M. Laurati, Model - Free Rheo - AFM Probes the Viscoelasticity of Tunable DNA Soft Colloids, *Small* 15(42) (2019) 1904136. <https://doi.org/10.1002/sml.201904136>
- [60] S.E. Cross, Y.-S. Jin, J. Rao, J.K. Gimzewski, *Nanomechanical analysis of cells from cancer patients, Nano-Enabled Medical Applications*, Jenny Stanford Publishing 2020, pp. 547-566.
- [61] C.F. Guimarães, L. Gasperini, A.P. Marques, R.L. Reis, The stiffness of living tissues and its implications for tissue engineering, *Nature Reviews Materials* 5(5) (2020) 351-370. <https://doi.org/10.1038/s41578-019-0169-1>
- [62] Y. Javanmardi, H. Colin-York, N. Szita, M. Fritzsche, E. Moeendarbary, Quantifying cell-generated forces: Poisson's ratio matters, *Communications physics* 4(1) (2021) 237. <https://doi.org/10.1038/s42005-021-00740-y>
- [63] F. Wottawah, S. Schinkinger, B. Lincoln, R. Ananthakrishnan, M. Romeyke, J. Guck, J. Käs, Optical rheology of biological cells, *Physical review letters* 94(9) (2005) 098103. <https://doi.org/10.1103/PhysRevLett.94.098103>
- [64] S. Kwon, W. Yang, D. Moon, K.S. Kim, Comparison of cancer cell elasticity by cell type, *Journal of Cancer* 11(18) (2020) 5403. <https://doi.org/10.7150/2Fjca.45897>
- [65] A. Rubiano, D. Delitto, S. Han, M. Gerber, C. Galitz, J. Trevino, R.M. Thomas, S.J. Hughes, C.S. Simmons, Viscoelastic properties of human pancreatic tumors and in vitro constructs to mimic mechanical properties, *Acta biomaterialia* 67 (2018) 331-340. <https://doi.org/10.1016/j.actbio.2017.11.037>

- [66] C. Alibert, B. Goud, J.B. Manneville, Are cancer cells really softer than normal cells?, *Biology of the Cell* 109(5) (2017) 167-189. <https://doi.org/10.1111/boc.201600078>
- [67] O.S. Qureshi, H. Bon, B. Twomey, G. Holdsworth, K. Ford, M. Bergin, L. Huang, M. Muzylak, L.J. Healy, V. Hurdwar, An immunofluorescence assay for extracellular matrix components highlights the role of epithelial cells in producing a stable, fibrillar extracellular matrix, *Biology open* 6(10) (2017) 1423-1433. <https://doi.org/10.1242/bio.025866>
- [68] N.V. Kosheleva, Y.M. Efremov, P.I. Koteneva, I.V. Ilina, I.M. Zurina, P.Y. Bikmulina, A.I. Shpichka, P.S. Timashev, Building a tissue: Mesenchymal and epithelial cell spheroids mechanical properties at micro-and nanoscale, *Acta Biomaterialia* 165 (2023) 140-152. <https://doi.org/10.1016/j.actbio.2022.09.051>
- [69] F. Di Lorenzo, J. Hellwig, R. von Klitzing, S. Seiffert, Macroscopic and microscopic elasticity of heterogeneous polymer gels, *ACS macro letters* 4(7) (2015) 698-703. <https://doi.org/10.1021/acsmacrolett.5b00228>
- [70] Z.I. Kalcioğlu, R. Mahmoodian, Y. Hu, Z. Suo, K.J. Van Vliet, From macro-to microscale poroelastic characterization of polymeric hydrogels via indentation, *Soft Matter* 8(12) (2012) 3393-3398. <https://doi.org/10.1039/C2SM06825G>